OPEN ACCESS
IOP Publishing
Journal of Optics
J. Opt. **16** (2014) 114005 (15pp)
doi:10.1088/2040-8978/16/11/114005

Invited Article

Multipole analysis of unidirectional light scattering from plasmonic dimers

E Poutrina[1,2] **and A Urbas**[1]

[1] Air Force Research Laboratories, 3005 Hobson Way, Wright Patterson, OH 45433, USA
[2] UES, Inc, 4401 Dayton-Xenia Rd, Dayton, OH 45432, USA

E-mail: ekaterina.poutrina.ctr.ru@us.af.mil

Received 22 June 2014, revised 15 August 2014
Accepted for publication 26 August 2014
Published 3 November 2014

Abstract

We analyze unidirectional scattering produced by sub-wavelength plasmonic dimers formed by two silver strips separated by a thin dielectric spacer and embedded in a uniform dielectric medium. Achieving the Kerker condition, which requires matching the strengths of the electric and magnetic-type contributions of the same multipolar order, is possible with such structures for both forward and backward unidirectional scattering by matching the geometric shape-leveraged resonant magnetic dipolar response with the off-resonant electric dipolar contribution. However, unidirectionality is strongly affected by coupling between the two elements in the dimer structure, leading to the manifestation of the electric quadrupole response in the far field. We develop an approach allowing for an easy inverse scattering retrieval of various multipole contributions to the far-field pattern produced by this type of geometry. The retrieval shows unambiguously that the electric quadrupole response contributes up to 30% of the scattered far-field intensity, in addition to strong manifestation of both electric and magnetic dipolar modes. A modified condition for unidirectionality can be developed based on the principle that suppression of radiation in either the forward or backward direction can be achieved whenever the *combined* strength of multipolar modes of a *certain parity*, radiating along the propagation direction, matches that of an opposite parity, and noting that parities of electric and magnetic modes interchange with increasing multipole order. With this condition satisfied, unidirectionality of 26 dB/17 dB for forward/backward scattering, respectively, can be achieved with dimer geometries. We also perform a detailed quantitative analysis of scattering cross sections of dimer structures compared to those of Si and gold spheres, accounting for the actual material losses. We show that dimer structures allow for improving backscattering unidirectionality by 10 dB compared to what is achievable with Si spheres, owing to their reliance on off-resonant electric dipolar response; they also allow for a significant (below $\lambda/10$) reduction of the size of a unidirectionally scattering nanoelement.

Keywords: scattering, particles, multipole analysis, plasmonics, polarizabilities retrieval
PACS numbers: 42.25 Fx, 78.67-n, 12.25 Bs

(Some figures may appear in colour only in the online journal)

1. Introduction

Light interactions on the nanoscale continue to acquire increasing attention, being the keystone for numerous applications, ranging from nano-sensors and photovoltaics to logic components for integrated optics and quantum computing. The

growth of interest in this direction is supported by significant improvements in contemporary fabrication capabilities, as well as by a considerable advancement in computational resources. While providing a possible path for controlling light near an atomic-scale level, light manipulation at the nanoscale faces limitations unique to the microscopic nature of the processes involved. One of the major limiting factors is the reduction of the degree of coherence occurring with the interaction of even a highly coherent light beam with a nanoscale object [1] which results in a significant reduction of directionality control. While focusing and re-routing of the light are routine procedures with macroscopic optics, diffraction dominates at the nanoscale. Control of the scattering response has been an active topic in the context of optical antennas [2–13]. In that vein, a logical path to regaining the control of directionality relies on exploiting the processes inherent to nanoscale interactions, such as interference effects between multipole modes of the electromagnetic field produced within a scattering event.

Unidirectional scattering from magneto-electric nanoparticles can be achieved when matching electric and magnetic polarizabilities of the scattering nanoelement, either with the same or the opposite signs [14–17]. With this condition satisfied, the electromagnetic waves emanating from the orthogonal, spatially superimposed electric and magnetic dipoles induced in the nanoelement by the external field interfere constructively in either the forward or backward direction, while being suppressed in the opposite direction. The particular direction of constructive interference is defined by the relative signs of electric and magnetic polarizabilities of the nanoelement, with the forward (backward) unidirectionality achieved when matching the two types of polarizabilities with the same (opposite) signs. Matching polarizabilities in the above way, or, more generally, matching the electric (a_l) and magnetic (b_l) coefficients up to an lth order in the multipole expansion of the field scattered from the nanoparticle, $a_l = \pm b_l$, is known as the Kerker condition [14].

We would like to note upfront that, while there is no limit on the strength of directionality for scattering in the forward direction, there is a fundamental limitation imposed by the optical theorem [18] preventing an ideal backward unidirectional scattering situation [15, 17]. The theorem states that extinction cross section (sum of absorption and scattering cross sections) is a function of the portion of light scattered in the forward direction. Hence, a complete cancelation of scattering in the forward direction would assume no scattering overall according to power conservation considerations. The theorem however does not prevent minimizing the scattering in the forward direction by interferometrically suppressing the field quadrature oscillating in phase with the incident field that does not contribute to extinction [15]. As a result, a pronounced unidirectionality in the backward direction can be achieved while maintaining a small but nonzero forward scattering amplitude, even when accounting for realistic losses in a nanoelement [19].

Since no natural materials are known that would exhibit electric and magnetic dipole transitions of a similar strength in the visible range (with magnetic ones usually being significantly weaker, even when pronounced), practical implementation of the above concept usually relies on leveraging the geometric shape-based magnetic response of nanoelements. Unidirectional response based on matching the dipolar polarizabilities of high-index dielectric nanospheres, such as Si or Ge, has been analyzed theoretically [20–22] and demonstrated experimentally both in the microwave [23] and in the visible range [24]. A detailed theoretical analysis has also been performed for other, mostly spherical nanoelements and their arrangements [25–30].

However, while matching directly the strengths of multipolar coefficients of electric and magnetic modes of the same order ($a_l = \pm b_l$) definitely leads to a unidirectional scattering response, a combination of multipolar modes of different orders can interact in more complicated ways leading to a similar result. A pronounced unidirectionality based on the interplay of both electric and magnetic dipolar and quadrupolar modes in a sphere of a moderate ($n \approx 2.4$) refractive index has been shown in [31]. Obtaining a preferential radiation direction with a single element possessing dipolar and quadrupolar modes has been realized in [32, 33]. While a strong forward/backward directionality of scattering obtained by a combination of magnetic dipolar and electric quadrupolar modes interacting with the electric dipolar response has been experimentally demonstrated in [34], implementing a split ring resonator-type geometry. The above examples are consequences of a more general concept, which we would like to state here and which constitutes one of the main points in the presented work: it can be intuitively expected that suppression of radiation in either the forward or backward direction can be achieved whenever the combined strength of multipolar modes of a certain parity, radiating along the propagation direction, matches that of the opposite parity. Since, for the same polarization, parities of electric and magnetic modes interchange when increasing the multipolar order l [35], a set of magnetic and electric modes of consecutive orders can act to counterbalance a combination of modes that get pronounced within a complimentary set of electric and magnetic modes. One example is the combination of an electric quadrupole and a magnetic dipole acting together to counterbalance the strength of an electric dipolar response. The concept can be extended further to include higher order multipoles, combining odd-order ($l = 1, 3, \ldots$) magnetic with even-order electric modes to counterbalance a combined action of modes pronounced within the complimentary set.

The above condition is relaxed compared to Kerker's, as it does not require a strict matching, or even the simultaneous manifestation of the multipoles of the same order. It is also more favorable for practical implementations, since most nanoelements possessing a geometric shape-leveraged magnetic dipolar response would simultaneously exhibit an electric quadrupolar mode, and possibly higher-order resonances. The latter situation is the case for most nanoparticles that exceed the static approximation [18] limit. More importantly, the strength of the electric quadrupole mode is related to the strength of field gradients within the nanoelement [35]. Such field gradients can be induced by 'coupling resonances' in nano-elements of a non-uniform composition. Since coupling resonances are capable of providing field enhancements orders of magnitude stronger than those achievable with an isolated uniform element [36], quadrupole response can

become dominant, or at least provide a considerable portion of the total far-field response. This can be the case even in extremely small but non-uniform nanoelements, that would otherwise fall into the static approximation limit and exhibit predominantly an electric dipole resonance. Thus, reliance on multipolar interference in such a generalized sense not only expands the degrees of freedom for practical implementation of unidirectional scatterers, but also suggests a path for developing such scatterers with a considerably reduced size. The latter, in turn, creates a path for achieving a high back-scattering unidirectionality, which requires the use of nanoelements small compared to the wavelength due to limitations imposed by the optical theorem [15].

In that vein, the dimer geometry is the simplest example incorporating the concepts above. In our previous work [19], we have demonstrated a possibility of achieving a strong (up to 25 dB) unidirectionality with dimer structures composed of two metal strips separated by a thin layer of a dielectric. Here, we develop the retrieval procedure allowing for the analysis of multipolar contributions into scattering from this and similar geometries, taking steps towards an analytical design of non axi-symmetric geometries with a unidirectional scattering response. We use the performed retrieval to demonstrate the above concepts of achieving strong forward/backward unidirectionality by combining dipolar and higher order multipolar contributions of the same parity; as well as achieving such a response from considerably (less than $\lambda/10$) subwavelength structures. The paper is organized as follows. The retrieval procedure is developed in section 2. In section 3, we test the retrieval method and the accuracy of our simulations by comparing the numerical scattering cross sections and the retrieved polarizabilities with those obtained by Mie theory in the case of spheres. We also present several observations in this section regarding the unidirectional response achievable with high-index dielectric spheres. We perform polarizability retrieval for dimers in section 4, providing the detailed quantitative analysis of multipolar contributions into the unidirectional scattering response produced with such geometries. We compare the unidirectional response from dimers with that achieved with high-index dielectric spheres, and perform a brief analysis of the change in the relative contribution of various multipolar modes, the unidirectionality strengths, and the scattering and extinction cross sections when changing the material parameters of the spacer layer in the dimer geometry.

2. Inverse scattering retrieval of dimer polarizabilities

The geometry and spectral response of the dimer structure are shown in figure 1. Here and further, we use the finite elements method incorporated within the COMSOL Multiphysics (www.comsol.com) commercial software package for performing these simulations. The geometry parameters are indicated on the figure. Air is assumed for the surrounding medium. The lower-frequency resonance ($\lambda = 769$ nm), characterized by the presence of the circulating displacement current (shown with arrows on the inset), is regularly associated with magnetic-type response [38–40], while the spectral position of the second resonance ($\lambda = 440$ nm) corresponds to that of a single wire of the same length, indicating the manifestation of electric dipolar-type resonant response of the dimer structure associated with that of a single wire at this wavelength [19]. As we have recently shown [19], the geometry is capable of producing a strongly pronounced unidirectional scattering of incident light in either the forward or the backward direction. An example of such a response for the spectral positions corresponding to the peaks of the unidirectionality strength at 751 nm and 789 nm is shown in figures 1(c) and (d). Unidirectionality is assumed to result from matching the strengths of the resonant magnetic-type (odd-parity in electric field) response at 770 nm with its off-resonant electric (even-parity) counterpart. Since magnetic polarizability changes sign at the resonance at 770 nm, switching from backward to forward scattering occurs when passing the 'magnetic' resonance moving to longer wavelengths.

We are aiming now at identifying the multipolar moments contributing to the produced far field pattern. It will be seen, in particular, that the odd-parity resonance at 770 nm has comparable contributions from both the magnetic dipolar and the electric quadrupolar modes. Below we summarize the description of electromagnetic modes that are expected to provide the strongest contribution to the scattered far-field produced by this and similar dimer geometries, aiming at the possibility of retrieving the polarizabilities of the dimer associated with these modes.

2.1. Dipolar modes

Consider a plane wave incident on a dimer element oriented transverse to the propagation direction, as shown in figure 1. Assuming the induced electric and magnetic dipoles are superimposed in space at the origin of the *xyz*-coordinate system, the electric far field radiated by a set of dipoles of moments $\mathbf{p} = \mathbf{p}_0 e^{-i\omega t}$ and $\mathbf{m} = \mathbf{m}_0 e^{-i\omega t}$ in vacuum is given by

$$\mathbf{E}^{el} = -\frac{e^{ikr}}{4\pi\epsilon_0}\left(\frac{\omega}{c}\right)^2 \frac{1}{r^3}\mathbf{r}\times\mathbf{r}\times\mathbf{p}_0, \tag{1a}$$

$$\mathbf{E}^{m} = -\frac{e^{ikr}}{4\pi}\sqrt{\frac{\mu_0}{\epsilon_0}}\left(\frac{\omega}{c}\right)^2 \frac{1}{r^2}\mathbf{r}\times\mathbf{m}_0, \tag{1b}$$

where the superscripts indicate the field scattered by electric and magnetic dipoles, r is the length of the radius-vector from the dipole location to the observation point, and the time harmonic factor has been omitted. The induced dipole moments are related to the electric $\overline{\overline{\alpha^e}}$ and magnetic $\overline{\overline{\alpha^m}}$ polarizability tensors of the dimer as $\mathbf{p}_0 = \varepsilon_0 \overline{\overline{\alpha^e}}\mathbf{E}_0$ and $\mathbf{m}_0 = \overline{\overline{\alpha^m}}\mathbf{H}_0$. In the latter expressions, $\mathbf{E}_0 = \left(E_{x0}, 0, 0\right)^T$ and $\mathbf{H}_0 = \left(0, E_{x0}/\eta, 0\right)^T$ are the vector amplitudes of the incident field, with $\eta \equiv \sqrt{\mu_0/\epsilon_o}$ denoting the free space impedance.

For a nanoelement exhibiting no optical activity, it is reasonable to assume the induced electric and magnetic

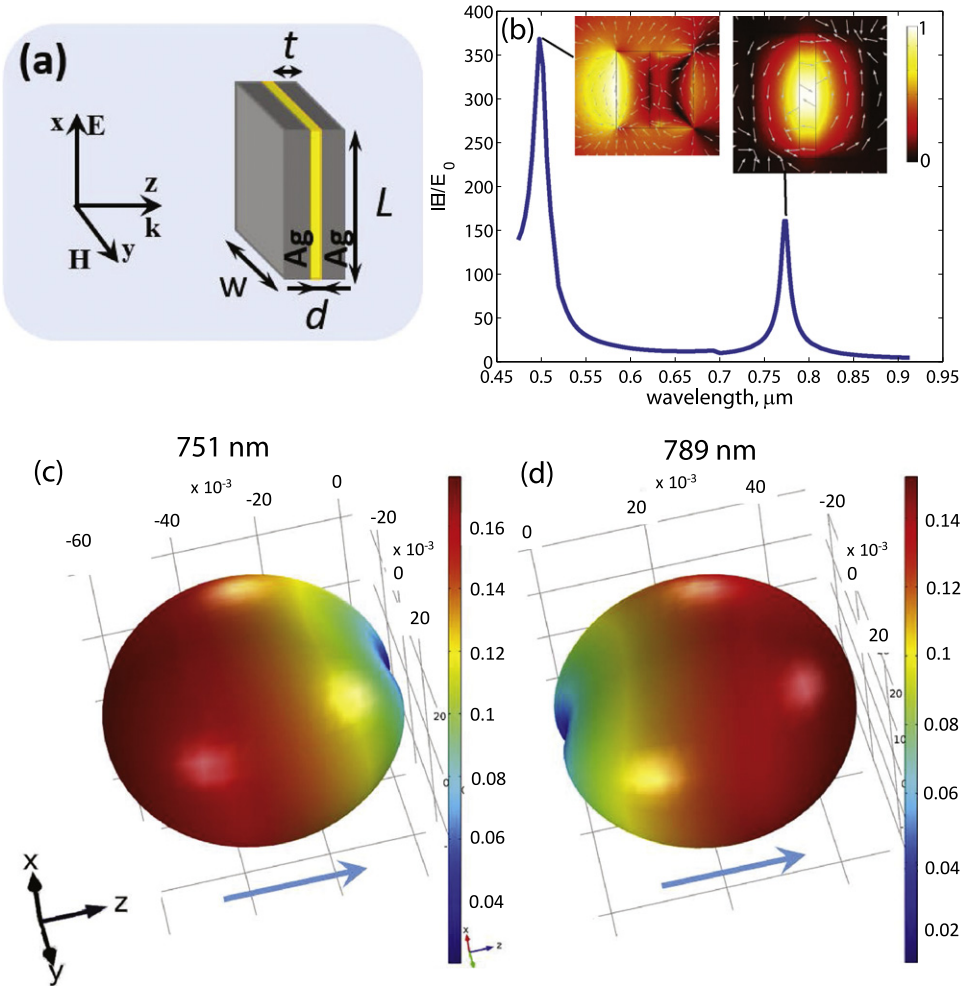

Figure 1. (a) Dimer geometry and orientation. Parameters used in (b) and (c): $L = w = 69$ nm, $t = 30$ nm, $d = 9$ nm, the spacer is Al_2O_3. Silver dielectric function follows the data in [37]. (b) Spectral dependence of field enhancement within the dimer. *Insets*: total magnetic near field distribution (*color plots*) and the direction of the total electric near field (*arrows*) within the '*xz*' cross-section, for the two resonant positions (440 nm and 769 nm). (c), (d) Differential scattering cross sections at the spectral positions corresponding to peaks of the unidirectional response. *Blue* arrows show the propagation direction of the incident field.

dipoles to be oriented along the corresponding vectors of the incident field. For the coupled wire structure shown in figure 1(a) that results in $\mathbf{p}_0 = \left(p_x, 0, 0\right)^T$ and $\mathbf{m}_0 = \left(0, m_y, 0\right)^T$ for the components of the induced electric and magnetic dipole moments, respectively. The Cartesian components of the scattered electric far field resulting from the combination of such *x*-oriented electric and *y*-oriented magnetic dipoles are as follows

$$E_x^{el+m} = \frac{k^2}{4\pi}\frac{e^{ikr}}{r}\left[\frac{1}{\epsilon_0}p_x\left(\sin^2\theta\sin^2\varphi + \cos^2\theta\right) + \eta m_y\cos\theta\right], \quad (2a)$$

$$E_y^{el+m} = -\frac{k^2}{4\pi}\frac{e^{ikr}}{r}\frac{1}{\epsilon_0}p_x\sin^2\theta\sin\varphi\cos\varphi, \quad (2b)$$

$$E_z^{el+m} = \frac{k^2}{4\pi}\frac{e^{ikr}}{r}\left[-\frac{1}{\epsilon_0}p_x\sin\theta\cos\theta\cos\varphi - \eta m_y\sin\theta\cos\varphi\right], \quad (2c)$$

where θ and φ are the angles with respect to *z*- and *x*-axes, respectively, in the standard spherical coordinates notation, and $k \equiv \omega/c$ is the wave vector. Similar expressions can be written for dipoles of other orientations if they happen to be induced in the nanoelement.

We will assume for now no optical activity is exhibited by the structures considered; we verify this assumption later in section 2 when performing a numerical analysis of the scattered far field pattern. In this case, the far field amplitudes of electric and magnetic dipolar modes are decoupled in the *xy* plane ($\theta = 90°$) and, if also no higher-order multipoles contribute to scattering into the *xy* plane, can be retrieved from the numerical values of $E^{el+m}(\theta = 90°, \phi = 0°)$ and

$E^{el+m}(\theta = 90°, \phi = 90°)$, respectively, using equation (2). For convenience, we write the explicit expressions for scattering into the three Cartesian planes below.

1. *XY* plane ($\theta = 90°$)

$$E_x^{xy^{el+m}} = \frac{k^2}{4\pi}\frac{e^{ikr}}{r}\left[\frac{1}{\varepsilon_0}p_x \sin^2\varphi\right], \tag{3a}$$

$$E_y^{xy^{el+m}} = \frac{k^2}{4\pi}\frac{e^{ikr}}{r}\left[-\frac{1}{\varepsilon_0}p_x \sin\varphi\cos\varphi\right], \tag{3b}$$

$$E_z^{xy^{el+m}} = \frac{k^2}{4\pi}\frac{e^{ikr}}{r}\left[-\eta m_y \cos\varphi\right]. \tag{3c}$$

2. *XZ* plane ($\varphi = 0°$)

$$E_x^{xz^{el+m}} = \frac{k^2}{4\pi}\frac{e^{ikr}}{r}\left[\frac{1}{\varepsilon_0}p_x \cos\theta + \eta m_y\right]\cos\theta, \tag{4a}$$

$$E_y^{xz^{el+m}} = 0, \tag{4b}$$

$$E_z^{xz^{el+m}} = \frac{k^2}{4\pi}\frac{e^{ikr}}{r}\left[-\frac{1}{\varepsilon_0}p_x \cos\theta - \eta m_y\right]\sin\theta. \tag{4c}$$

3. *YZ* plane ($\varphi = 90°$)

$$E_x^{yz^{el+m}} = \frac{k^2}{4\pi}\frac{e^{ikr}}{r}\left[\frac{1}{\varepsilon_0}p_x + \eta m_y \cos\theta\right], \tag{5a}$$

$$E_y^{yz^{el+m}} = 0, \tag{5b}$$

$$E_z^{yz^{el+m}} = 0. \tag{5c}$$

One can easily verify that the presence of either electric or magnetic dipolar modes produced by dipoles oscillating in directions other than those along the incident field vectors would change the far field angular distribution in the *xy* plane from the one given by equation (3). The validity of the assumption of no additional dipolar modes being induced can then easily be verified by reconstructing the angular distribution of the far field in the *xy* plane from the retrieved values of electric and magnetic dipolar amplitudes according to equation (3) and comparing the result with the numerically produced shape. The dipolar amplitudes retrieved in the above way can then be used for predicting scattering into the *xz* and *yz* planes arising from dipolar contributions with the help of equations (4) and (5).

The Kerker condition [14], ideally, corresponds to the case when $\mathrm{Re}\,(\frac{1}{\varepsilon_0}p_x) = \pm\,\mathrm{Re}\,(\eta m_y)$ and $Im\left(\frac{1}{\varepsilon_0}p_x\right) = Im\,(\eta m_y)$. (We assume here passive materials such that the imaginary parts of the polarizabilities are always positive, leading to the positive imaginary parts of the induced dipole moments p_x and m_y.) As seen from equations (4) and (5), in this case scattering in the backward direction ($\theta = \pi$) is completely suppressed when matching the electric and magnetic dipolar amplitudes with the same sign, while scattering in the forward direction ($\theta = 0$) is minimized when the real parts of dipolar amplitudes are matched with the opposite sign. One can also immediately see the consequence of the optical theorem mentioned in the introduction, which prevents a complete suppression of scattering in the forward direction: the signs of the imaginary parts remain the same (positive) for lossy elements, preventing a complete matching of the two types of the polarizabilities with the opposite signs required in the backward scattering case.

2.2. Coupled dipoles response

If the dipolar response were the only one pronounced in the dimer structure, unidirectionality in the *xz* and *yz* planes could be predicted by retrieving the dipolar polarizabilities from scattering in the *xy* plane as discussed in the previous section and then finding the response in the other two planes using equations (4) and (5). However, while it is reasonable to assume no dipoles other than those co-polarized with the incident field are induced in the nanoelement, for any dimer structure, the presence of two closely spaced elements suggests a possibility of coupling between the dipolar modes of each of these elements forming either an electric quadrupole-type response (in the case of, e.g., the 'π' phase difference between the two otherwise equal dipolar modes) or other coupled-dipoles radiation pattern; the particular field pattern depends on the relative phases of the dipolar modes induced in the two elements. We will assume now no multipolar contributions to the far field other than those arising from the above coupled-dipole response are produced (in addition to the dipolar modes) within the geometry with the excitation as in figure 1. This assumption is justified later in section 4.

The far field pattern $\mathbf{E}^q$ radiated by the combination of two dipoles of amplitude $\tilde{\mathbf{p}}_0$ each, having a relative phase difference δ, and shifted by small distances $\pm a$ from the origin along the propagation direction direction (z), can formally be found as

$$\begin{aligned}\mathbf{E}^q &= \tilde{\mathbf{E}}^{el}(0)e^{-i\mathbf{k}\cdot\mathbf{a}} + \tilde{\mathbf{E}}^{el}(0)e^{i\delta}e^{+i\mathbf{k}\cdot\mathbf{a}}\\ &= \tilde{\mathbf{E}}^{el}(0)e^{i\frac{\delta}{2}}\left[e^{-i\frac{\delta}{2}}e^{-ika\cos\theta} + e^{+i\frac{\delta}{2}}e^{+ika\cos\theta}\right]\\ &= \tilde{\mathbf{E}}^{el}(0)e^{i\frac{\delta}{2}}2\cos\left(ka\cos\theta + \frac{\delta}{2}\right).\end{aligned} \tag{6}$$

In the above expression, $\tilde{\mathbf{E}}^{el}(0) \equiv -\frac{e^{ikr}}{4\pi\varepsilon_0}\left(\frac{\omega}{c}\right)^2\frac{1}{r^3}\mathbf{r}\times\mathbf{r}\times\tilde{\mathbf{p}}_0$ is the far field of the dipolar mode of each cut-wire that would be produced if the wire were located at the origin. Equation (6) is reasonably accurate for dipole separations such that $ka \leqslant 2\pi$. We assumed the same value of amplitude $\tilde{\mathbf{p}}_0$ for each of the dipolar modes, noting the identical lengths of the two wires considered here. Note that a 'tilde' sign was used over the dipole amplitude above to distinguish the effective dipolar mode associated with the single wire from the dipolar response of the dimer as a whole used in equation (1).

The particular phase induced in a dipolar particle in the proximity of another dipolar oscillator, with both elements placed in air, had been analyzed in detail in [10, 11] and shown to depend strongly on the near-field interaction between the dipoles. Here, the relative phase δ is aimed to be retrieved from the scattered far field pattern. Our goal, however, is to retrieve the amplitude and phase of the resulting

coupled dipoles response as a whole, if such response gets pronounced in the far field, rather than assign specific values to parameters $\tilde{\mathbf{p}}_0$ and a used in the formal derivation in equation (6), as discussed in more detail below and in section 4.

It is instructive to consider a few particular values of the relative phase difference between the dipolar modes: that of current oscillations in phase in the two wires ($\delta = 0$), oscillations with the opposite phases ($\delta = \pi$), and the intermediate case $\delta = \pi/2$. For the above three cases, equation (6) simplifies to

$$\mathbf{E}^q\Big|_{\delta=0} = 2\tilde{\mathbf{E}}^{el}(0)\cos(ka\cos\theta), \tag{7a}$$

$$\mathbf{E}^q|_{\delta=\pi/2} = \tilde{\mathbf{E}}^{el}(0)\mathrm{e}^{\mathrm{i}\frac{\pi}{4}}\sqrt{2}\,[\cos(ka\cos\theta) - \sin(ka\cos\theta)], \tag{7b}$$

$$\mathbf{E}^q|_{\delta=\pi} = -\tilde{\mathbf{E}}^{el}(0)2\imath\sin(ka\cos\theta) \approx -\tilde{\mathbf{E}}^{el}(0)2\imath ka\cos\theta. \tag{7c}$$

In the latter expression we additionally assumed the separation distance to be small such that $ka \ll 1$, which is consistent with our geometry. As seen from equation (7), for $\delta = 0$ or $\delta = \pi$ the angular distribution of the scattered field is always symmetric with respect to the origin, including symmetry between the forward and backward scattering directions. Between these two cases, for small values of separation distance ($ka \ll 1$), oscillations in phase ($\delta = 0$) result in a doughnut-shaped angular pattern oriented in a yz plane, similar to that of a single oscillating dipole but squeezed along the z axis by a factor of $\cos(ka\cos\theta)$. Out of phase oscillations ($\delta = \pi$), on the other hand, produce a figure-eight pattern oriented along the z axis, such that no scattering occurs in the xy ($\theta = 90°$) plane.

Any value of the induced relative phase δ other than 0 or π would introduce an asymmetry between the forward and the backward scattered fields. Additionally, for a fixed value of the phase difference $\delta \neq 0, \pi$, the angular distribution would strongly depend on the particular separation distance a between the dipoles, oscillating between the forward and backward scattering when changing the separation. In particular, for $\delta = \pi/2$, backward scattering would be completely suppressed if such a phase difference could be achieved with dipole separation of $ka = 3\pi/4$, while suppression in the forward direction would occur if the $\delta = \pi/2$ were achieved with $ka = \pi/4$ separation.

We remind the reader however that, as discussed in [10, 11] and in the previous paragraphs, the induced relative phase δ itself depends on the separation between wires and is aimed to be retrieved from the far field distribution pattern. The above discussion, nevertheless, suggests that the relative phase values of $\delta = 0$ or π can unambiguously be distinguished from any other value by the symmetric shape of the far field pattern with respect to the origin; further distinguishing between the '0' and 'π' values can be made by the presence or absence, respectively, of scattering into the xy plane. Moreover, for the particular structure considered here, one can expect a priori the opposite phase of dipolar oscillations in the two wires in the spectral region around the magnetic dipolar resonance, due to the pronounced circulating displacement current running through the cut wires in this case, leading to the value of $\delta \approx \pi$. The limiting value of the relative phase $\delta = \pi$ for small separation distances was also shown analytically in [10, 11], with both elements embedded in air.

As mentioned in the beginning of this section, the coupled dipoles response is that of a quadrupole-type in the case of the phase difference of π between the dipolar modes; in particular, for the excitation and the coordinate choice as in figure 1, it corresponds to the 'xz' Cartesian component of the quadrupole tensor, with the diagonal components vanishing assuming such charge distribution. Using equation (1a) in equation (7c), and accounting for the small separation between wires ($ka << 1$), the Cartesian components of the far field produced by such quadrupole interaction can then be written as following

$$E_x^q = \frac{k^2}{4\pi\epsilon_0}\frac{\mathrm{e}^{\mathrm{i}kr}}{r}q_{xz}^{el}\left(\sin^2\theta\sin^2\varphi + \cos^2\theta\right)\cos\theta, \tag{8a}$$

$$E_y^q = -\frac{k^2}{4\pi\epsilon_0}\frac{\mathrm{e}^{\mathrm{i}kr}}{r}q_{xz}^{el}\sin^2\theta\sin\varphi\cos\varphi\cos\theta, \tag{8b}$$

$$E_z^q = -\frac{k^2}{4\pi\epsilon_0}\frac{\mathrm{e}^{\mathrm{i}kr}}{r}q_{xz}^{el}\sin\theta\cos^2\theta\cos\varphi, \tag{8c}$$

where we defined $q_{xz}^{el} \equiv -2\mathrm{i}ka\tilde{p}_x$. Note that in our notation q_{xz} differs by the factor of $\mathrm{i}k/6$ from what is regularly used [35]. We choose however the normalization as in equation (8) for the sake of relating the scattered field $\mathbf{E}_{\mathrm{far}}^{\mathrm{sc}}$ to the scattering amplitude $\mathbf{A}$ in a general manner for all multipole moments as

$$\mathbf{E}_{\mathrm{far}}^{\mathrm{sc}} = \mathbf{E}^{el+m} + \mathbf{E}^q \equiv \frac{\mathrm{e}^{\mathrm{i}kr}}{r}\mathbf{A}E_0, \tag{9}$$

where both $\mathbf{E}_{\mathrm{far}}^{\mathrm{sc}}$ and $\mathbf{A}$ are assumed to be in the far field zone.

The retrieval of the multipoles contributing to the far fields would be simplified in the above case of $\delta = \pi$, since, according to the above discussion, such quadrupole-type response would not produce any scattering into the xy plane. The dipolar modes can then be retrieved in the way discussed in the previous section, while the amplitude of the quadrupolar response can be found from the difference between the actual far field scattered into the xz plane and that expected to be produced by the dipolar contributions alone, as summarized in the following section.

2.3. Polarizabilities retrieval

According to equations (3a), (3c), and (9), with the assumptions of the only induced dipolar modes being those along the incident field vectors and no higher-order moments contributing to scattering into the xy plane, one can find the electric and magnetic dipolar polarizabilities by probing the scattering amplitude in the directions ($\theta = 90°$, $\varphi = 90°$) and

($\theta = 90°$, $\varphi = 0°$) as following

$$\alpha_{xx}^{el} = \frac{4\pi}{k^2} A(\theta = 90°, \varphi = 90°), \tag{10a}$$

$$\alpha_{yy}^{m} = \frac{4\pi}{k^2} A(\theta = 90°, \varphi = 0°). \tag{10b}$$

The accuracy of the above assumptions can then be verified by reconstructing the angular distributions of the Cartesian components of the scattering amplitude in the xy plane using equation (3) and comparing with the numerically produced shapes. The retrieved polarizabilities can be further used for predicting the angular distribution of scattering into the xz and yz planes coming from dipolar contributions using equations (4) and (5). Finally, anticipating the π phase difference between the dipolar oscillation in the two wires, the amplitude $\mathbf{A}^q$ of the electric quadrupolar contribution can be found as the difference between the numerical value of the amplitude actually scattered in the forward ($\theta = 0°$) direction and the one that would have resulted from the sum of the dipolar contributions alone as $\mathbf{A}^q(\theta = 0°) = \mathbf{A}(\theta = 0°) - [\mathbf{A}(\theta = 90°, \varphi = 90°) + \mathbf{A}(\theta = 90°, \varphi = 0°)]$. For the single component of the quadrupole tensor considered, we can further define quadrupolar polarizability α^q in a similar way through $q_{xz}^{el} \equiv \epsilon_0 \alpha^q E_0$, with α^q being formally substituted for $-2ika\tilde{\alpha}_{xx}$. It is then related to $\mathbf{A}$ through equations (8) and (9)

$$\alpha^q = \frac{4\pi}{k^2} \mathbf{A}^q(\theta = 0°). \tag{11}$$

Thus, the dipolar and quadrupolar polarizabilities of the dimer element with orientation as in figure 1 are expected to be found by determining the magnitude and phase of the scattering amplitude in the three orthogonal directions: ($\theta = 90°$, $\varphi = 0°$), ($\theta = 90°$, $\varphi = 90°$), and ($\theta = 0°$), for the incident electric field polarization along ($\theta = 90°$, $\varphi = 0°$).

We note that, while an example of a cut wire pair is considered in the present study, the analysis is relevant to other geometries that utilize the excitation of a magnetic dipolar mode owing to the displacement current circulating in the plane of incidence; such situation would be the case for most dimer-type geometries oriented transverse to the propagation direction and having the two elements in the dimer spaced along the propagation direction.

2.4. Relation to numerical procedures

The far field scattering amplitude $A(\hat{\mathbf{r}}_0)$ in a given direction $\hat{\mathbf{r}}_0$ can numerically be found by integrating the scattered near fields $\mathbf{E}$ and $\mathbf{H}$ over an arbitrary surface S enclosing the scattering objects using the Stratton–Chu formula [35]

$$\mathbf{A}(\hat{\mathbf{r}}_0) = -\frac{1}{E_0}\frac{ik}{4\pi}\hat{\mathbf{r}}_0 \times \int_S \left[\mathbf{n} \times \mathbf{E} - \eta \hat{\mathbf{r}}_0 \times (\mathbf{n} \times \mathbf{H})\right] \times e^{ik\mathbf{r}'\cdot\hat{\mathbf{r}}_0} dS', \tag{12}$$

where $\mathbf{n}$ is a normal to surface S and $\hat{\mathbf{r}}_0$ is a unit vector along the direction of interest.

In addition to polarizability retrieval, the knowledge of the scattering amplitude allows us to calculate the numerical values of the scattering cross sections in a usual manner. According to the optical theorem [18], the extinction cross section C_{ext} can be found as a function of the far-field amplitude in the forward direction ($\theta = 0°$ for the incident wave traveling along z) as following

$$C_{\text{ext}} = \frac{4\pi}{k} \text{Im}\left(\mathbf{A}|_{\theta=0}\right). \tag{13}$$

The absorption cross section can be calculated by normalizing the absorbed power P_{abs} by the intensity of the incident field

$$C_{\text{abs}} = P_{\text{abs}}/I_0, \tag{14}$$

where, in turn, P_{abs} can be found by integrating the heat losses over the volume of the particle: $P_{\text{abs}} = \frac{1}{2}\int_\Omega \text{Re}\left\{\mathbf{J}^* \cdot \mathbf{E}\right\} dV$. Finally, the scattering cross section is obtained as the difference between the extinction and absorption

$$C_{\text{sca}} = C_{\text{ext}} - C_{\text{abs}}. \tag{15}$$

The accuracy of numerical procedures can be verified by comparing the numerical results for the above quantities with those found by Mie theory for some regular geometric shapes. We perform such validation in the next section using the examples of a Si and a gold sphere, at the same time providing a quantitative insight into the unidirectional response produced by the Si sphere.

3. Validation: unidirectional scattering from Si sphere

The extinction, absorption, and scattering cross sections calculated numerically according to section 2.3 in comparison with the results from Mie theory for Si and gold nanoparticles of radiuses $R = 60$ nm and 30 nm, respectively, are shown in figure 2 . Depicted are scattering efficiencies, defined as the cross sections given by equations (13)–(15) normalized by the geometric cross section of the particle, i.e. $\sigma_{\text{ext}} \equiv C_{\text{ext}}/\pi R^2$, etc. There is a perfect agreement in all cases. For the theory curves, we accounted for 30 orders in the Mie theory expansion; only the first two orders, however, give a significant contribution to the total result, as can be seen from figure 3(a) which shows the spectral dependence of the polarizabilities for the Si sphere. As seen from that figure, for wavelengths larger than about 440 nm, the response of the Si sphere is largely dominated by dipolar contributions, such that the scattered far field $\mathbf{E}_{\text{far}}^{\text{sc}}$, with good accuracy, can be represented by the sum of electric and magnetic dipolar modes described by equations (3)–(5). This allows the use of equation (10), which assumes no higher than the dipolar contribution in the directions used in the retrieval $\left(A^q\big|_{\substack{\theta=90° \\ \varphi=0°,90°}} = 0\right)$, for finding the dipolar polarizabilities of the sphere within this frequency range. The resulting polarizabilities are shown as circles in figure 3(a), in a good agreement with the Mie results.

For $\lambda \approx 488$ nm and 560 nm (λ_1 and λ_2, respectively, in figure 3(a)) the real parts of electric and magnetic

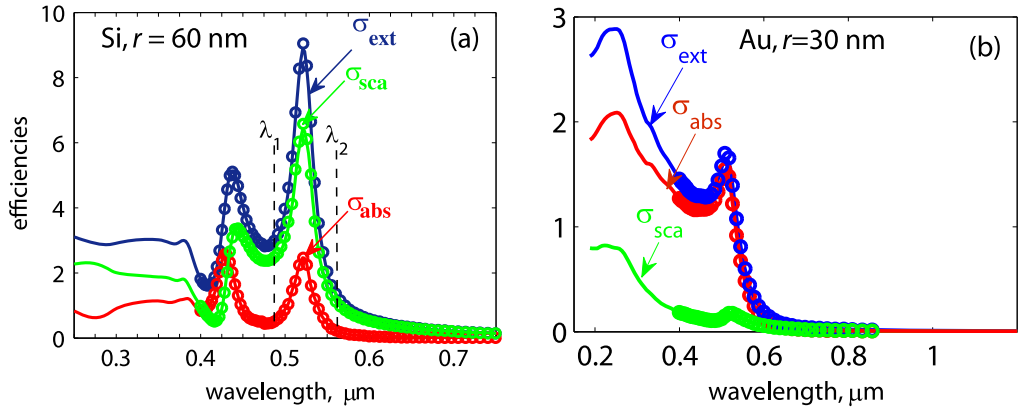

Figure 2. Extinction, absorption, and scattering cross sections for (a) Si nanoparticle of 60 nm radius and (b) gold sphere of 30 nm radius. In all cases, circles are the numerical results and lines are Mie theory. The dielectric function of Si follows that of crystalline Si in [41]. Gold dielectric function follows the data in [37].

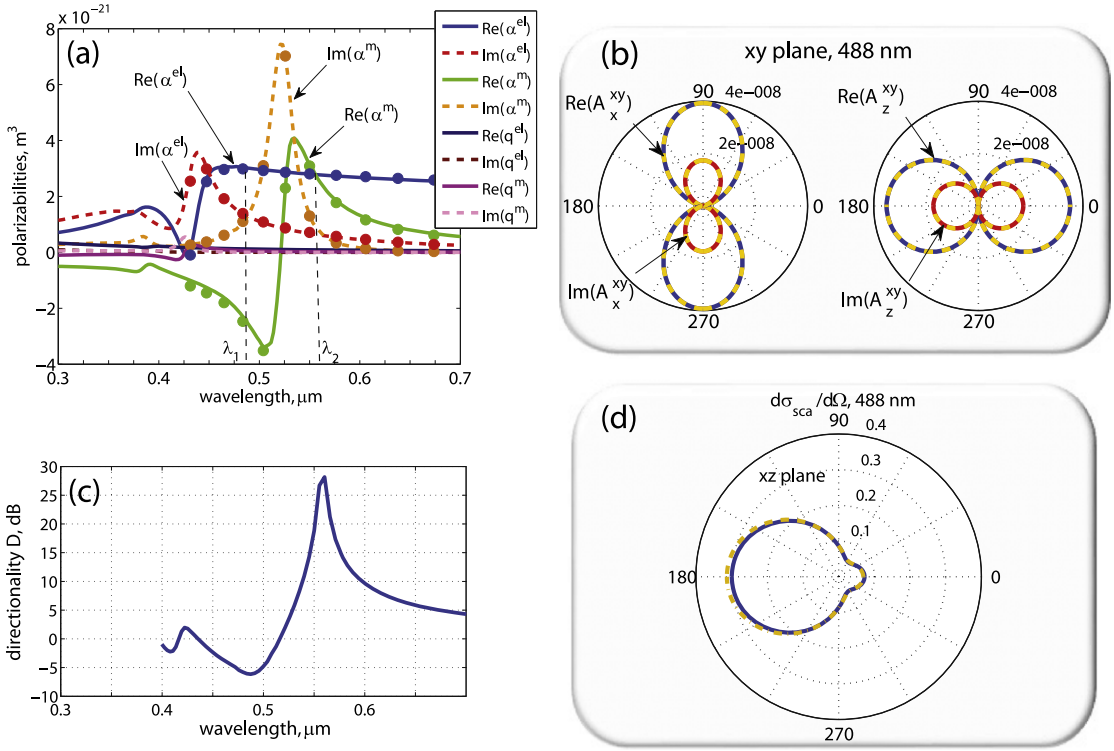

Figure 3. (a) Polarizabilities of the Si sphere from figure 2 calculated with Mie theory (*lines*) and retrieved using equation (10) (*circles*). (b) Angular distribution of scattering amplitude in the *xy* plane. *Blue* and *red*: numerical results. *Dashed yellow*: calculated from the retrieved polarizabilities using equation (3). (c) Directionality ratio for the sphere. (d) Differential scattering cross section for scattering into the *xz* plane, obtained numerically (*blue*) and from equation (4) (*yellow*). Predominantly dipolar modes contributed to the far field response at the wavelength considered.

polarizabilities match with the opposite and the same signs, thus approximately satisfying the second and the first Kerker conditions, respectively. Hence, one can expect a pronounced backward and forward unidirectional scattering response, respectively, in the two cases. We plot the real and imaginary parts of the scattering amplitude in the *xy* plane and the differential scattering cross section $\left(\mathrm{d}\sigma_{\mathrm{sca}}/d\Omega \equiv \frac{1}{(\pi R^2)}\frac{|\mathbf{A}|^2}{k^2}\right)$ in the *xz* plane in figures 3(b) and (d), respectively, for the first of the above wavelengths. Note that the integral of the $\mathrm{d}\sigma_{\mathrm{sca}}/\mathrm{d}\Omega$ over the surface of a unit sphere surrounding the particle, taken for each spectral position, would reproduce the spectral dependence for the total scattering cross section shown in figure 2(a). The analytical curves, shown by dashed lines, are calculated using equations (3) and (4), respectively. There is an excellent agreement between the numerical the theoretical curves in the *xy* plane which represents scattering produced predominantly by the dipolar modes, showing once again the accuracy of the simulations and the retrieval, as well as validating the assumption of no contribution from the dipolar oscillations induced in the directions other than those along the incident field. For the *xz* plane, a small difference between the analytical yellow

dashed line, representing dipolar contribution into the xz plane and the actual scattering amplitude indicates an additional scattering from higher order multipoles into this plane. The discrepancy is however negligible (as might be expected due to the dominance of the dipolar terms at this wavelength, according to figure 3(a)), while accounting for these responses would require a retrieval procedure different from that of section 2.3, due to the different (diagonal) electric quadrupolar moment in the case of a sphere, and also a small manifestation of a magnetic quadrupole, and we will not focus on it here.

In addition to numerical validation of the accuracy of the numerical and retrieval procedures, we would like to use the above quantitative analysis to draw attention to some features that are common in the case of a unidirectional response from a dielectric sphere, irrespective of the particular parameters used in figures 2 and 3. The spectral dependence of the directionality of the response D, calculated as the ratio (in dB) of the differential scattering cross sections in the forward and backward directions, $D \equiv 10\log_{10}\left(|A|^2_{\theta=0^\circ}/|A|^2_{\theta=180^\circ}\right)$, is shown in figure 3(c). As expected, the peaks correspond to the two wavelengths providing the match of the two polarizabilities, λ_1 and λ_2. Considering the limitations on the backscattering unidirectionality imposed by the optical theorem [15, 17], it is somewhat counterintuitive that the absolute value of the scattering cross section for the backscattering peak is, in fact, about twice larger than that for one in forward scattering. This can be explained by a rather weak unidirectionality for the backscattering that is about 6 dB according to figure 3(c). Both features, a rather low backscattering unidirectionality and a higher absolute value of the cross section for backscattering than for the forward scattering, are quite general in the case of a unidirectional response achieved with a dielectric sphere. Similar low backscattering ratios persist in the simulations for spheres of other diameters, as well as in the experimental demonstration in [24]. It can be explained by the fact that the unidirectional operation utilizes the near-resonant values of both electric and magnetic polarizabilities as following. Backscattering operation requires opposite signs of the real parts of electric and magnetic polarizabilities. Since the magnetic dipolar resonance is regularly red-shifted with respect to the electric one [42], the spectral position for the backscattering peak is in between the two resonances. Due to both resonances being still close to one another in the case of a dielectric sphere, imaginary parts of the polarizabilities are relatively high at this spectral location, preventing a strong backscattering unidirectionality, as explained in section 2.1. On the other hand, the absolute value of the scattering cross section is larger for the backscattering 'peak' due its 'double-resonant' location, than for the forward one, which is shifted to the opposite side of the magnetic resonance and further away from the electric resonance peak.

We will see in the next section that the directionality in the backward scattering case can be improved by about 10 dB by using dimer structures, while also allowing for a considerable reduction of the nanoelement size. We proceed now to the analysis of such unidirectional operation obtained with cut-wire geometry.

4. Multipole analysis of unidirectional scattering from cut-wire dimers

Polarizabilities for the cut-wire structure demonstrated in figure 1, retrieved using equations (10) and (11), are presented in figure 4(a), showing a strong contribution from the electric quadrupolar response, with the electric quadrupole and magnetic dipole resonances centered at the same spectral position. As a verification, the angular distribution of the field scattered into the xy plane, found both numerically and by using the retrieved dipolar polarizabilities in equation (3), is shown in figure 4(b) for one of the spectral positions. The exact agreement of the two results validates the assumptions of no dipolar moments being induced in the dimer in the directions other than along the incident field vectors, as well as no contributions for scattering into the xy plane produced by higher order multipoles. A similar comparison of the numerical and the retrieved angular dependencies for the quadrupole response, the latter obtained by using the retrieved quadrupolar polarizability in equation (8), is plotted in figure 4(d) for the same wavelength. A similar excellent agreement validates the assumptions made in deriving equation (8), in particular the negligible conribution of other higher-order multipoles to the far field response, as well as a close to π phase difference between the dipolar responses of the two wires. We observed a similar perfect overlap of numerical and analytical curves for all spectral positions in figure 4(a), as well as for all other cut-wire structures we've considered. (We note that a minor asymmetry in the angular shape of the quadrupole response can be seen for somewhat larger structures/separations, indicating a small deviation of the relative phase from π, similar to the results in [11] for the near-field dipoles interaction in air. The asymmetry, however, is within few percent of the quadruple amplitude and is negligible to unpronounced in the combined far field pattern, for all dimer structures we've considered that exhibited a noticeable unidirectional response.)

As seen from figure 4(a), the Kerker condition, $\alpha^{el} = \pm\alpha^{m}$ is achieved for the real parts of electric and magnetic dipolar polarizabilities at 758 nm and 780 nm. However, the presence of the quadrupolar term can be expected to modify the far-field directionality ratio from what would have been achieved with the dipolar responses only. We note that Kerker condition, $a_l = b_l$, is essentially a request for matching the polarizabilities of the same order but of an opposite parity, such as those of electric and magnetic dipoles. However, the parities of multipole fields interchange with increasing the multipolar order [35]. Hence, if several multipolar orders are simultaneously pronounced, a set of magnetic and electric modes of consecutive orders, radiating along the propagation direction, can act on counterbalancing a combination of modes that get pronounced in a complimentary set of electric and magnetic modes, suppressing radiation in either forward or backward direction. In the present example, electric quadrupole and magnetic dipole both radiate along the propagation axis and

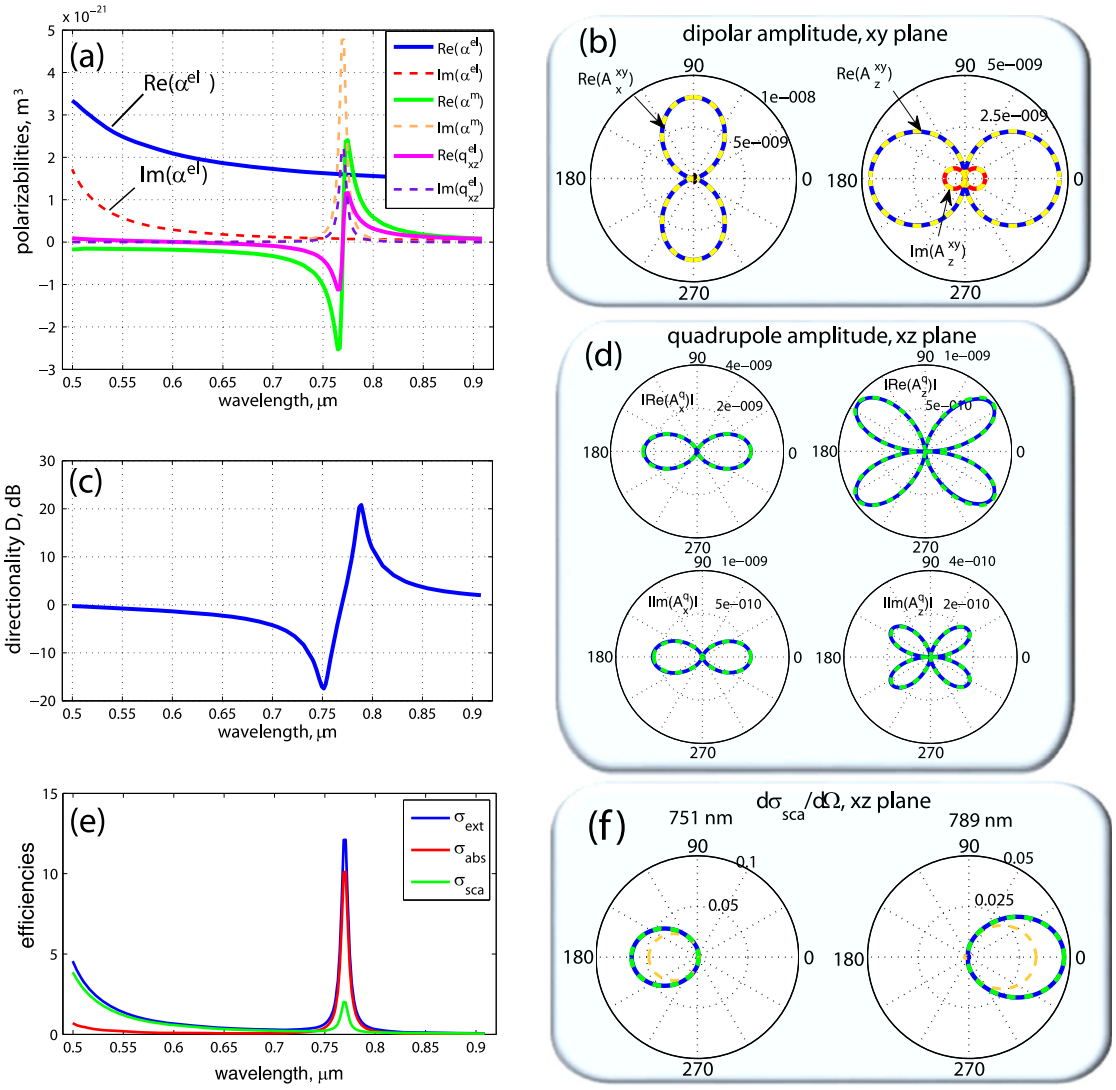

Figure 4. (a) Retrieved polarizabilities for the dimer with the geometry from figure 1. (b) Angular distribution of scattering amplitude in the *xy* plane for the same dimer structure. *Blue* and *red*: numerical results. *Dashed yellow*: calculated from the retrieved polarizabilities using equation (3). (c) Spectral dependence of the directionality ratio. (d) Angular distribution of the quadrupole amplitude scattered into the *xz* plane. *Solid blue*: numerical result obtained by subtracting the dipolar contributions from the scattered far field. *Dashed green*: fit using equation (8). (e) Extinction, absorption, and scattering cross sections for the above dimer structure, calculated as described in section 2.3. (f) Differential scattering cross section for scattering into the *xz* plane for the peak unidirectionality spectral positions. *Solid blue*: numerical result. *Dashed green*: theoretical fit accounting for both dipolar and quadrupolar response. *Dashed yellow* shows the result that would be obtained with only the dipolar contributions.

are expected to act together counterbalancing the electric dipolar response.

To better illustrate the concept, we plot in figure 5(a) the 3D distributions of the norm of the far field for the modes assumed to contribute to the combined far field pattern in the case of the current geometry, as well as for a magnetic quadrupole mode. The patterns are simulated using arbitrary electric, magnetic, and two closely-spaced ($ka = 0.1$) oppositely oscillating dipoles, ensuring the conditions $-\frac{1}{\epsilon_0}p_x + \eta m_y + \frac{1}{\epsilon_0}q^{el} = 0$ and $\frac{1}{\epsilon_0}p_x - \eta m_y + \eta q^m = 0$ for figures (b) and (c), respectively, in each case assuming 25% of the scattered far-field intensity arises due to the quadrupolar term. As seen from figure 5(a), both magnetic dipole and electric quadrupole produce odd-type (in electric field) patterns, while an even-type response is generated by the electric dipole and magnetic quadrupole terms. As a result, radiation can be interferometrically suppressed on one side of the scatterer, as shown in figures 5(b) and (c). One can see also that, in agreement with the shape predicted by equation (7*c*), no contribution to scattering into the *xy* plane is produced by the quadrupolar response. The situation is, however, not unique and a similar effect can be achieved (in a different geometry) with, e.g., a magnetic quadrupole field adding to an electric dipolar response, counterbalancing the strength of a magnetic dipole. While it would be beyond the scope of this paper to consider another geometry in detail, we present the general idea in the case of a magnetic quadrupole contribution in figure 5(b). A larger number of multipoles can similarly be included.

As such, for the geometry considered here, we can expect the directionality to be strongly pronounced at the spectral

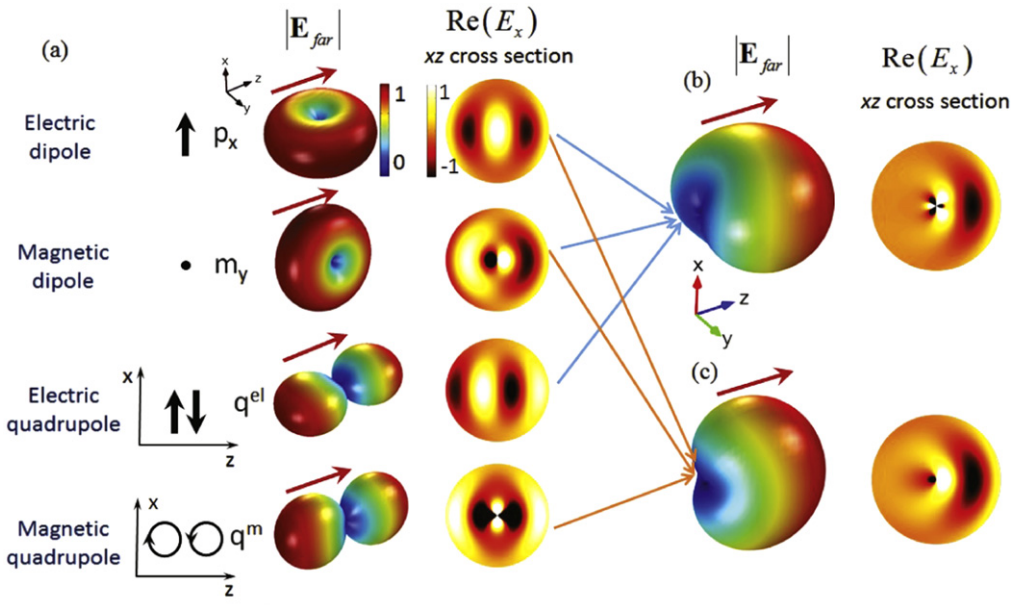

Figure 5. Illustration of the combined action of dipolar and quadrupolar modes in achieving a unidirectional response. (a) *Left*: Angular distribution of the far field for the participating modes. *Right*: *xz* cross section of the electric field amplitude for each mode, showing alternating parities of dipolar and quadrupolar modes. (b) and (c) Far field pattern and the *xz* cross section of electric field amplitude produced due to the interference of several multipolar modes, as shown by blue and brown arrows. Red arrow indicates the propagation direction of the incident beam.

positions where $\mathrm{Re}\,(\alpha^m + \alpha^q) = \pm\,\mathrm{Re}\,(\alpha^{el})$, and the polarizabilities are related to the dipolar and quadrupolar contributions according to the notation in section 2.

The directionality ratio D for the structure presented in figure 1 is shown in figure 4(c). As expected, the directionality peaks at 751 nm and 789 nm for the backward and forward scattering directions, respectively, in agreement with the positions where the combined response of magnetic dipole and quadrupole moments matches that of electric dipole, according to figure 4(a). The scattering amplitude in the *xz* plane for the above two wavelengths is plotted in figure 4(f), showing a perfect agreement between the numerical and the retrieved spectra. The dashed yellow curve shows the response that would have been achieved at these spectral locations with only the dipolar contributions. There is, of course, a noticeable discrepancy between the dipolar-only prediction and the actual result, indicating that the directionality is improved by about 30% due to the quadrupolar contribution. More interestingly, the improvement occurs for both forward and backward directions. While an interferometric suppression of radiation due to cooperative action of magnetic dipole the electric quadrupole can be expected according to figure 5, it is due to the fact that both the magnetic dipole and the electric quadrupole acquire resonance at the same spectral position ($\lambda = 770$ nm) and change the phase of oscillation once passing the resonant point, that the improvement in directionality occurs for both directions. The coincidence of the spectral positions of the two resonances can be understood as a consequence of both magnetic and quadrupole terms being induced by the same displacement current circulating within the dimer in the *xz* plane, for the type of the geometry considered. The situation should however be common for other types of dimer structures having a pronounced *xz* component of the quadrupole mode, such as two dipolar particles spaced along the propagation direction.

Finally, we would like to note a strong unidirectionality achieved in both forward and backward directions, with more than 10 dB improvement in the backward case, compared to the Si sphere in the previous section. Moreover, it is achieved with an ultra-small particle of 69 nm size—the geometric area less than half of that of the Si sphere considered. The improvement results from operating in the off-resonant region of the electric dipolar response, where the imaginary part of the dipolar resonance is reduced. Since a large spectral separation between electric and magnetic-type resonances is common for cut-wire geometries [19], such improvement would generally occur for most dimer structures of this type.

The improvement, however, comes at the expense of a reduced scattering cross section, as seen from figure 4(e). Nevertheless, the scattering efficiency is still almost an order of magnitude larger than that of a gold sphere of a similar geometric cross section (figure 2(b)), while a comparison to the Si sphere is somewhat unfair due to an almost twice larger geometric size of the latter; Si sphere of a similar small size would, however, not be able to produce a unidirectional response, due to the weak magnetic dipolar mode [42] (the reason we implemented a larger diameter).

There are several ways for improving the cross section, such as: the use of somewhat larger elements; the increase of the spacer thickness (the latter would reduce both the real and the imaginary parts of the effective index of the metal-dielectric-metal nanowavegude formed between the metal strips), the use of a lower index spacer (leading to a similar effect as increasing the spacer thickness), and certainly the

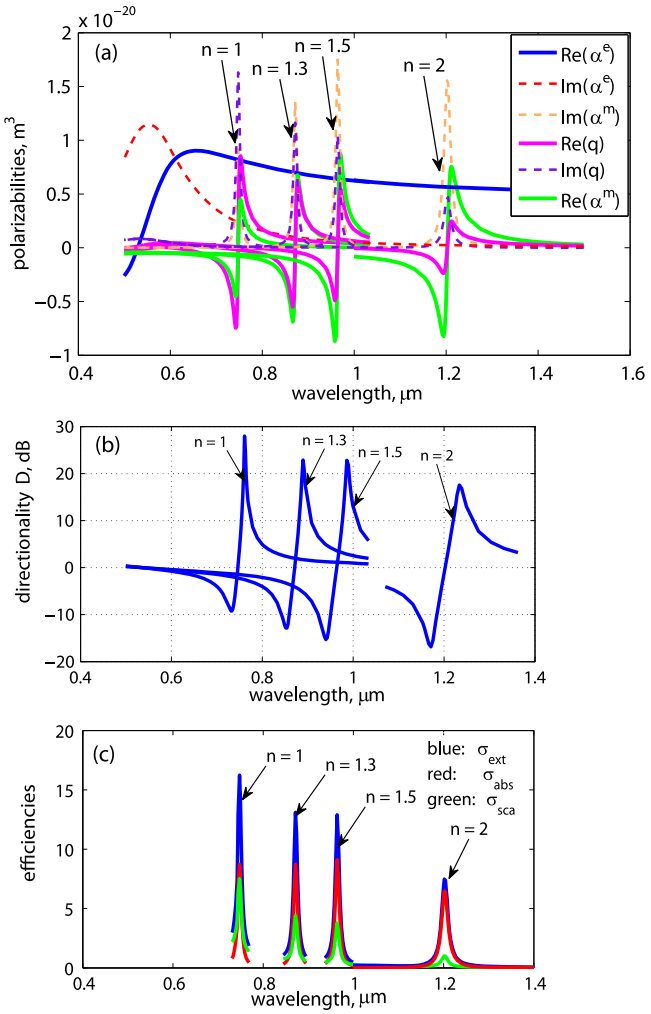

Figure 6. Variation of (a) polarizabilities, (b) directionality ratios, and (c) cross sections when changing the refractive index of the spacer from $n = 1$ to $n = 2$. The rest of the parameters remained the same as follows: $L = 120$ nm, $t = 30$ nm, $d = 11$ nm.

use of lower loss materials. While there is no goal here in the analysis of all the possibilities, we provide some guidance below on the change of the response when gradually reducing the refractive index of the spacer.

We consider a somewhat larger dimer structure of $L = 120$ nm and make a gradual change of the refractive index of the spacer from $n = 2$ to that of an air, while keeping the rest of the parameters the same. The resulting cross sections, directionality ratios, and the retrieved polarizabilities are shown in figure 6.

As seen in figure 6(a), the relative contribution of the quadrupolar mode is reduced when increasing the spacer index, while the magnetic dipolar mode grows, thus making the total contribution of the odd-parity (in electric field) modes relatively unchanged. The magnetic dipolar mode eventually reaches maximum strength around $n \approx 1.5$, and gradually decreases with a further increase of the spacer index and other parameters fixed. The particular index value providing such an optimum strength of the magnetic dipolar mode ensures achieving the maximum resonant enhancement of the magnetic field within the dimer volume, and is specific to the particular dimer geometry and material parameters, as had been discussed in more detail in [19]. In particular, such factors as the area encompassed by the circulating displacement current loop versus the total 'xz' cross section area, as well as losses induced in the effective metal-dielectric-metal waveguide formed by the dimer structure, affect the optimal value of the spacer index. The reduction of the quadrupolar strength, on the other hand, can intuitively be understood as the consequence of the reduced non-uniformity of the dimer structure with the increased index; decreasing non-uniformity reduces gradients of the electric field within the nanoelement, leading to the reduction in the quadrupole strength.

The directionality ratios (figure 6(b)) initially grow noticeably for the backward response, owing to a spectral shift further away from the electric resonance located at $\lambda = 550$ nm. This shift leads to a strong reduction of the imaginary part of the electric dipolar response, resulting in higher backscattering unidirectionality, as we discussed earlier. The magnetic resonance however gradually broadens due to increased effective losses for a higher-index spacer. That leads to a stronger mismatch between the imaginary parts of magnetic and electric dipolar modes, leading to the reduction of the unidirectionality in the forward direction. The directionality is quite strong, however, in all cases, varying between 28 dB and 18 dB for the forward direction and between about 10–16 dB for the backward scattering. We would like to note here that, even though a similar response is produced with an air spacer, the mechanism of directionality here is different from that in an optical Yagi–Uda design where a similar response is obtained by achieving a phase delay between the neighboring elements in a structure. In that sense, Yagi–Uda is closer to the situation described by equation (7*b*), which produces an asymmetric (between the forward and backward directions) radiation pattern due to the phase delay between the two wires. For the structures considered here, however, the two elements of a dimer are assumed to be in the near fields of each other, such that the phase difference is always close to π, leading to a symmetric angular shape of the radiated power (and odd electric field parity).

Finally, the cross sections for all configurations are shown in figure 6(c). A noticeable decrease of the extinction cross section is seen with increasing index; it is reduced almost by half with the spacer index increase from $n = 1$ to $n = 2$. The reduction, for the most part, is again due to a shift away from the electric dipolar resonance. As shown, the imaginary part of the electric dipolar mode reduces rapidly between the spectral positions corresponding to magnetic and quadrupole resonances for $n = 1$ and $n = 1.5$. Since, according to optical theorem, it is the imaginary part of the scattered field that contributes to extinction (equation (13)), the latter is also noticeably reduced (with the reduction being somewhat counterbalanced by slightly increasing contributions from magnetic and quadrupolar modes). Due to the radiative nature of the dipolar mode, the reduction of the extinction cross section comes mostly at the expense of the scattering cross

section, with absorption acquiring less of a change. Also, while the geometric size of the dimer element stays the same, its size relative to the (magnetic/quadrupolar) resonant wavelength is reduced owing to the red-shift of the resonant position with increased spacer index. This also contributed to reduction of the extinction cross section. We note also that the agreement of numerical and analytical angular distributions was perfect, similar as in figure 4, for all geometries and spectral positions considered.

5. Conclusions

In conclusion, we emphasized that suppression of scattering in either forward or backward directions can be achieved whenever the combined strength of multipolar modes of a certain parity, radiating along the propagation direction, matches that of the opposite parity. Since, for the same polarization, parities of electric and magnetic modes interchange when increasing the multipolar order, a set of magnetic and electric modes of consecutive orders can act on counterbalancing a combination of modes that are pronounced within a complimentary set of electric and magnetic modes. Examples of this situation include a combined action of a magnetic dipole and an electric quadrupole counterbalancing the electric dipolar response, with a proper choice of the dipolar orientations and the quadrupolar tensor component; or, alternatively, a combination of an electric dipole and a magnetic quadrupole counteracting the magnetic dipolar mode; higher multipolar orders can similarly be included. Moreover, while the manifestation of higher-order multipoles is regularly associated with nanoelements of a relatively large size, the dimensions of a nanoelement exhibiting such a response can be drastically reduced utilizing structures with a non-uniform material composition, such as dimer geometries. As a result, relying on multipolar interference in such a generalized manner, compared to matching the strengths of electric and magnetic multipoles of the same order, not only expands the degrees of freedom for practical implementation of unidirectional scatterers, but also suggests a path for developing such scatterers with a considerably reduced size.

We demonstrated the above concepts numerically by utilizing a geometry composed of two metal strips separated by a thin dielectric layer and oriented transversally to the propagation direction. A 69 nm size unit, operating around 770 nm wavelength, was presented. We derived an approach allowing for an easy retrieval of multipolar polarizabilities associated with such structures. The retrieval shows unambiguously that almost 100% of the contribution to the far field in these structures comes from the combination of electric and magnetic dipolar modes, oriented transversally to the propagation direction and orthogonally to each other, and an electric quadrupolar mode arising due to an off-diagonal component of the quadrupole tensor, with the quadrupolar response contributing up to 30% of the total far field amplitude. The derived approach can be used for similar dimer geometries composed of two dipolar elements spaced closely along the propagation direction.

We tested the accuracy of our numerical simulations and the retrieval procedure by comparing the scattering cross sections and the dipolar polarizabilities for spherical nanoparticles obtained using Mie theory with those calculated numerically and retrieved using the presented approach. The comparison showed an excellent agreement between the two results. While performing such a quantitative analysis, we emphasized a few observations which are rather general in the case of a unidirectional scattering achieved with high-index dielectric spheres. In particular, the backscattering unidirectionality is relatively low, of the order of 6 dB or less, with this type of geometry. This results from the relatively close spectral positions of electric and magnetic dipolar modes in the case of spheres, leading to relatively high imaginary parts of both types of polarizabilities at the optimal spectral position for backscattering; the latter is necessarily located in between the two resonances. The achievable forward scattering unidirectionality is comparably higher, due to the spectral location of the forward-scattering peak on the opposite side of the magnetic dipolar resonance, further away from the electric one. Such 'double-resonant' nature of the backscattering response also leads to a somewhat counterintuitive, in terms of the limitations due to optical theorem, result that the absolute value of the backscattering cross section, in the case of spheres, is regularly about twice as large as that of the forward scattering cross section. The result, however, is not surprising, noting the low directionality.

We demonstrated that backscattering directionality can be improved by about 10 dB with dimer structures, which utilize an off-resonant portion of the electric dipolar response. The unidirectionality of 26 dB/17 dB in the forward/backward direction is demonstrated numerically with the 69 nm dimer structure. The improvement, however, comes at the expense of reduced absolute values of scattering cross sections at the spectral regions allowing for a unidirectional scattering operation. Nevertheless, the overall scattering cross section is about an order of magnitude larger than that of a gold nanoparticle of a similar size.

As well, we've provided an insight into the change in the values of the extinction and scattering cross sections, of the directionality ratio, and of the induced multipolar polarizabilities when reducing the refractive index of the spacer layer from $n = 2$ to that of air, with other parameters unchanged, using an example of a dimer structure of a somewhat larger size (120 nm). The relative contribution of the quadrupole mode reduces with increasing spacer index, while the magnetic dipolar mode grows, eventually passing through a peak strength with the spacer index maximizing field enhancement of the magnetic resonant mode ($n \approx 1.5$ for the geometry in the present study). The change is accompanied by the red-shift of the magnetic/quadrupolar resonance away from the dipolar resonance. This leads to the increase in the backscattering unidirectionality, with a simultaneous decrease of the scattering amplitude. The overall directionality ratio stays strong throughout the

index change, with backscattering values varying between about 10 and 16 dB, while forward scattering achieving 28 dB values for $n = 1$ and gradually reducing to about 18 dB for $n = 2$, due to the broadening of magnetic dipolar mode.

The presented analysis and the retrieval approach can be used for further development of deeply subwavelength structures exhibiting a unidirectional scattering response for the numerous applications requiring the directional control of light on the nanoscale.

References

[1] Born M and Wolf E 1980 *Principles of Optics* (Cambridge: Cambridge University Press)

[2] Novotny L and van Hulst N F 2011 Antennas for light *Nature Photon.* **5** 83

[3] Li J, Salandrino A and Engheta N 2007 Shaping light beams in the nanometer scale: a Yagi–Uda nanoantenna in the optical domain *Phys. Rev.* B **76** 2454037

[4] Curto A G, Volpe G, Taminiau T H, Kreuzer M P, Quidant R and van Hulst N F 2010 Unidirectional emission of a quantum dot coupled to a nanoantenna *Science* **329** 930

[5] Kosako T, Kadoya Y and Hofmann H F 2010 Directional control of light by a nano-optical Yagi–Uda antenna *Nature Photon.* **4** 312

[6] Shegai T, Chen S, Miljkovic V D, Zengin G, Johansson P and Kall M 2012 A bimetallic nanoantenna for directional colour routing *Nat. Commun.* **2** 481

[7] Pakizeh T and Kall M 2009 Unidirectional ultracompact optical nanoantennas *Nano Lett.* **9** 2343

[8] King N S, Li Y, Ayala-Orozco C, Brannan T, Nordlander P and Halas N J 2011 Angle- and spectral-dependent light scattering from plasmonic nanocups *ACS Nano* **5** 7254

[9] Shegai T, Miljkovic V D, Bao K, Xu H X, Nordlander P, Johansson P and Kall M 2011 Unidirectional broadband light emission from supported plasmonic nanowires *Nano Lett.* **11** 706

[10] Bonod N, Devilez A, Rolly B, Bidault S and Stout B 2010 Ultracompact and unidirectional metallic antennas *Phys. Rev.* B **82** 115429

[11] Rolly B, Stout B, Bidault S and Bonod N 2011 Crucial role of the emitter-particle distance on the directivity of optical antennas *Opt. Lett.* **36** 3368

[12] Pakizeh T 2012 Unidirectional radiation of a magnetic dipole coupled to an ultracompact nanoantenna at visible wavelengths *J. Opt. Soc. Am.* B **29** 2446

[13] Lavasani A S H and Pakizeh T 2012 Color-switched directional ultracompact optical nanoantennas *J. Opt. Soc. Am.* B **29** 1361

[14] Kerker M, Wang D-S and Giles C L 1983 Electromagnetic scattering by magnetic spheres *J. Opt. Soc. Am.* **73** 765

[15] Alù A and Engheta N 2010 How does zero forward-scattering in magnetodielectric nanoparticles comply with the optical theorem? *J. Nanophotonics* **4** 041590

[16] Nieto-Vesperinas M, Saenz J J, Gomez-Medina R and Chantada L 2010 Optical forces on small magnetodielectric particles *Opt. Express* **18** 11428

[17] García-Cámara B, de la Osa R A, Saiz J M, González F and Moreno F 2011 Directionality in scattering by nanoparticles: Kerkers null-scattering conditions revisited *Opt. Lett.* **36** 728

[18] Bohren C F and Huffman D R 1983 *Absorption and Scattering of Light by Small Particles* (New York: Wiley)

[19] Poutrina E, Rose A, Brown D, Urbas A and Smith D R 2013 Forward and backward unidirectional scattering from plasmonic coupled wires *Opt. Express* **21** 31138

[20] Nieto-Vesperinas M, Gomez-Medina R and Saenz J J 2011 Angle-suppressed scattering and optical forces on submicrometer dielectric particles *J. Opt. Soc. Am.* A **28** 54

[21] Gomez-Medina R, Garcia-Camara B, Suarez-Lacalle I, Gonzalez F, Moreno F, Nieto-Vesperinas M and Saenz J J 2011 Electric and magnetic dipolar response of germanium nanospheres: interference effects, scattering anisotropy and optical forces *J. Nanophotonics* **5** 053512

[22] Garcia-Camara B, Gomez-Medina R, Jos Senz J J and Sepulveda B 2013 Sensing with magnetic dipolar resonances in semiconductor nanospheres *Opt. Express* **21** 23007

[23] Geffrin J M *et al* 2012 Magnetic and electric coherence in forward- and back-scattered electromagnetic waves by a single dielectric subwavelength sphere *Nat. Commun.* **3** 1171

[24] Fu Y H, Kuznetsov A I, Miroshnichenko A E, Yu Y F and Lukyanchuk B 2013 Directional visible light scattering by silicon nanoparticles *Nat. Commun.* **4** 1527

[25] Liu W, Miroshnichenko A E, Neshev D N and Kivshar Y S 2012 Broadband unidirectional scattering by magneto-electric core-shell nanoparticles *ACS Nano* **6** 5489

[26] Krasnok A E, Miroshnichenko A E, Belov P A and Kivshar Y S 2012 All-dielectric optical nanoantennas *Opt. Express* **20** 20599

[27] Rolly B, Stout B and Bonod N 2012 Boosting the directivity of optical antennas with magnetic and electric dipolar resonant particles *Opt. Express* **20** 20376

[28] Merchiers O, Moreno F, Gonzalez F and Saiz J M 2007 Light scattering by an ensemble of interacting dipolar particles with both electric and magnetic polarizabilities *Phys. Rev.* A **76** 043834

[29] Garcia-Camara B, Moreno F, Gonzalez F and Martin O J F 2010 Light scattering by an array of electric and magnetic nanoparticles *Opt. Express* **18** 10001

[30] Mulholland G W, Bohren C F and Fuller K A 1994 Light-scattering by agglomerates coupled electric and magnetic dipole method *Langmuir* **10** 2533

[31] Rolly B, Geffrin J-M, Abdeddaim R, Stout B and Bonod N 2013 Controllable emission of a dipolar source coupled with a magneto-dielectric resonant subwavelength scatterer *Sci. Rep.* **3** 3063

[32] Coenen T, Arango F B, Koenderink A F and Polman A 2014 Directional emission from a single plasmonic scatterer *Nat. Commun.* **5** 3250

[33] Krasnok A E, Filonov D S, Simovski C R, Kivshar Y S and Belov P A 2014 Experimental demonstration of superdirective dielectric antenna *Appl. Phys. Lett.* **104** 133502

[34] Hancu I M, Curto A G, Castro-Loìpez M, Kuttge M and van Hulst N F 2014 Multipolar interference for directed light emission *Nano Lett.* **14** 166

[35] Jackson J D 1967 *Classical Electrodynamics* (New York: Wiley) chapter 9

[36] Poutrina E, Ciracì C, Gauthier D J and Smith D R 2012 Enhancing four-wave-mixing processes by nanowire arrays coupled to a gold film *Opt. Express* **20** 11005

[37] Johnson P B and Christy R W 1972 Optical constants of the noble metals *Phys. Rev.* B **6** 4370

[38] Dolling G, Enkrich C, Wegener M, Zhou J F, Soukoulis C M and Linden S 2005 Cut-wire pairs and plate pairs as magnetic atoms for optical metamaterials *Opt. Lett.* **30** 3198

[39] Shalaev V M, Cai W, Chettiar U K, Yuan H-K, Sarychev A K, Drachev V P and Kildishev A V 2005 Negative index of refraction in optical metamaterials *Opt. Lett.* **30** 3356

[40] Cai W, Chettiar U K, Yuan H-K, de Silva V C, Kildishev A V, Drachev V P and Shalaev V M 2007 Metamagneticism with rainbow color *Opt. Express* **15** 3333

[41] Palik E D 1985 *Handbook of Optical Constants of Solids* (Boston: Academic)

[42] Garcia-Etxarri A, Gomez-Medina R, Froufe-Perez L S, Lopez C, Chantada L, Scheffold F, Aizpurua J, Nieto-Vesperinas M and Saenz J J 2011 Strong magnetic response of submicron silicon particles in the infrared *Opt. Express* **19** 4815